Spatial and energy resolution of electronic states by shot noise

E. S. Tikhonov [1,*] A. O. Denisov,[1,†] S. U. Piatrusha [1] I. N. Khrapach,[1,2,3] J. P. Pekola [4,2] B. Karimi [4]
R. N. Jabdaraghi,[4,5] and V. S. Khrapai[1,6]

[1]*Institute of Solid State Physics, Russian Academy of Sciences, 142432 Chernogolovka, Russian Federation*
[2]*Moscow Institute of Physics and Technology, 141700 Dolgoprudny, Russia*
[3]*Russian Quantum Center, 121205 Skolkovo, Moscow, Russia*
[4]*Pico group, QTF Centre of Excellence, Department of Applied Physics, Aalto University, FI-00076 Aalto, Finland*
[5]*VTT Technical Research Centre of Finland, P.O. Box 1000, FI-02044 VTT, Finland*
[6]*National Research University Higher School of Economics, 20 Myasnitskaya Street, Moscow 101000, Russia*

Shot-noise measurements are widely used for the characterization of nonequilibrium configurations in electronic conductors. The recently introduced quantum tomography approach was implemented for the studies of electronic wave functions of few-electron excitations created by periodic voltage pulses in phase-coherent ballistic conductors based on the high-quality GaAs two-dimensional electron gas. Still relying on the manifestation of Fermi correlations in noise, we focus on the simpler and more general approach beneficial for local measurements of energy distribution (ED) in electronic systems with arbitrary excitations with well-defined energies and random phases. Using biased diffusive metallic wire as a test bed, we demonstrate the power of this approach and extract the well-known double-step ED from the shot noise of a weakly coupled tunnel junction. Our experiment paves the way for local measurements of generic nonequilibrium configurations applicable to virtually any conductor.

Nanoscale temperature mapping and control of nonequilibrium configurations has attracted much interest recently. The prominent examples range from thermometry in a living cell [1] to thermal imaging of quantum systems [2] and nanoscale devices [3]. Along with direct thermal measurements and NVC- and SQUID-based thermometers [4], primary shot-noise thermometry is also attractive due to its self-calibrating nature [5,6]. Historically, it was first used for the study of hot-electron regimes in metallic resistors [7–9] and was later extended to primary electronic thermometry [5] and to the studies of graphene [10–15].

Shot-noise power of the current fluctuations S_I in a DC-biased two-terminal conductor, however, provides neither local nor energy resolution because random fluctuations of the occupation numbers of the electronic quantum states are averaged both in the energy interval where electron scattering is possible and along the length of the device [16]. This fundamental constraint set by current conservation [17] makes accessible only the device-averaged nonequilibrium noise temperature T_N. To gain further insight into the charge kinetics, one can measure the dynamical response of noise to an AC excitation [18–21] or implement the special design of the experiment to guide currents in a magnetic field [22].

Recently, shot noise was utilized to study electronic wave functions emitted by the time-dependent currents in a phase-coherent conductor [23,24]. Essentially, the implemented to-

mographic approach uses antibunching of fermions due to Pauli principle in the geometry of a beam splitter. So far, it has been used for characterization of excitations created by specific T-periodic identical voltage pulses. These excitations are a coherent superposition of single-particle eigenstates [25] with different energies in the range of $\sim \hbar/T$ with a spatial extension of $v_F T$. On the other hand, the fermionic system with arbitrary excitations with well-defined energies and random phases should rather be characterized by the energy distribution (ED). As we experimentally demonstrate below, an alternative approach [26], still relying on the manifestation of Fermi correlations in noise, is beneficial for its local measurements.

Up to now, ED measurements in mesoscale devices typically relied on the spectral sensitivity of the used detector. This spectral sensitivity inherent, e.g., to superconducting electrodes or quantum dots (QDs) with discrete electronic energy levels, allowed to use them as sensors for the measurements of ED inside current-driven mesoscopic metallic wires [27–29] and carbon nanotubes [30], and for the edge-channel spectroscopy in the integer quantum Hall regime [31,32]. In these experiments, EDs were obtained by measuring average current through the tunnel junction (TJ) and through the QD, respectively. As initially understood by Gramespacher and Büttiker [26], energy-resolved local information is accessible even without using any spectral-sensitive detector, being concealed in current fluctuations measured with a local probe rather than in the average current. In this case, energy sensitivity is provided solely by the Pauli exclusion principle, which couples EDs in the equilibrium reservoir and in the studied device in the expression for the

---

*tikhonov@issp.ac.ru
†Present address: Department of Physics, Princeton University, Princeton, New Jersey 08544, USA

shot noise. Note there is no external limiting energy scale in this approach besides bath temperature.

In this paper, we demonstrate experimental proof of principle of such local noise spectroscopy. To illuminate the main idea of the experiment, we first consider two electron reservoirs with EDs f_1 and f_2 coupled, for the moment, by a TJ with an energy-independent transmission probability. The average partial tunneling current in the energy strip $\delta\varepsilon$ from the ith to the jth reservoir for a single conduction channel is $\delta I_{i\to j} \propto f_i(1 - f_j)\,\delta\varepsilon$. The factors f_i and $(1 - f_j)$ are imposed by the Pauli exclusion principle. Still, the expression for the average partial tunneling current through the TJ $\delta I = \delta I_{1\to 2} - \delta I_{2\to 1} \propto (f_1 - f_2)\,\delta\varepsilon$ is identical to the classical case. However, the quasiparticle statistics is revealed in the fluctuations of currents $\delta I_{1\to 2}$ and $\delta I_{2\to 1}$, which add up in a Schottky-like manner to give the current noise spectral density: $\delta S_I = 2e[|\delta I_{1\to 2}| + |\delta I_{2\to 1}|] \propto [f_1 + f_2 - 2f_1 f_2]\,\delta\varepsilon$. This coupling of the EDs on the two sides of the TJ enables the energy resolution in the shot-noise measurement. Provided one takes into account the transmission eigenvalue distribution by the introduction of the Fano factor in the expression for the shot noise, the above reasoning applies for any multimode conductor with transport occurring at constant energy. Equally important, in the nonequilibrium configuration, zero average current through the conductor can coexist with its noise which by far exceeds the Johnson-Nyquist value. For the simplest case of a temperature difference across the conductor, this was recently demonstrated for InAs-nanowires [33] and for atomic scale junctions [34,35].

In the following, we will demonstrate the measurements of ED in micrometer-scale nonequilibrium metallic wires, see Fig. 1(a) for the sketch of the experiment setup. The sensor reservoir is described by the equilibrium ED $f_1 \equiv f_s = f_0(\varepsilon - eV, T_0)$, and the probed conductor locally by some nonequilibrium ED $f_2 \equiv f(\varepsilon)$. Here, $f_0(\varepsilon, T) = [\exp[\varepsilon/(k_B T)] + 1]^{-1}$ is the Fermi-Dirac (FD) distribution, V is the bias voltage across the TJ connecting the two reservoirs, and T_0 is the bath temperature. Changing V effectively scans f_s relatively to the studied nonequilibrium f, see Figs. 1(b) and 1(d). The current across the TJ is $I \propto \int [f_0(\varepsilon - eV) - f(\varepsilon)]\,\delta\varepsilon \propto V$, see Fig. 1(c). At the same time, the V-dependent contribution to the partial current noise spectral density $\delta S_I \propto f_0(\varepsilon - eV)[1 - 2f(\varepsilon)]\,\delta\varepsilon$ leads to the peculiar $S_I(V)$ dependence with

$$\frac{dS_I}{dV} \propto 1 - 2f(eV). \qquad (1)$$

Expression Eq. (1) is the essence of the local noise spectroscopy we develop here. Analogous expressions, already contained in the pioneering theory of the local noise probe [26], were later derived for the auto-correlation noise [36] and cross-correlation noise [37] in nonequilibrium Tomonaga-Luttinger liquids for studies of an AC-biased TJ [20], used for quantum tomography purposes [24] and for semiconducting nanowire-based local noise sensors [38,39]. For nonequilibrium $f(\varepsilon)$ with possibly many steplike features, each step is associated with the change of the slope in the $S_I(V)$ dependence. Below we explain the relation between these kinks and the local ED in the diffusive wire in the present experiment.
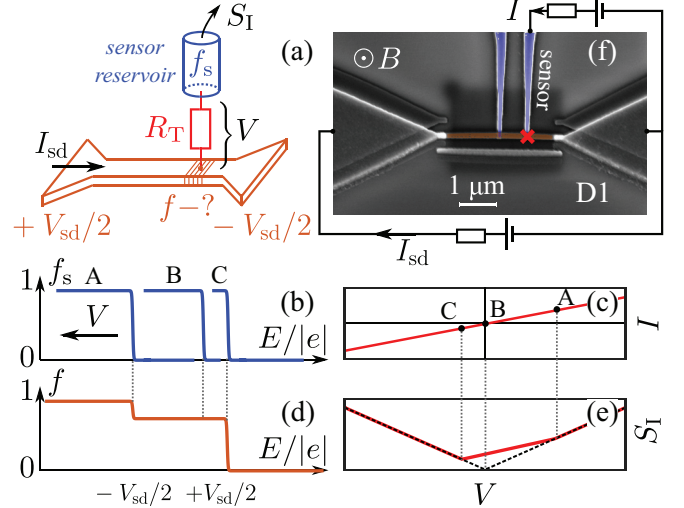

FIG. 1. (a) Schematic measurement setup. The central narrow wire is driven out of equilibrium with a transport current I_{sd}. Current fluctuations $S_I(V)$ are measured from the sensor reservoir which is tunnel coupled to the wire. (b), (d) ED in the sensor f_s and in the nonequilibrium wire in contact point f (in case of negligible inelastic scattering at $T = 0$) for $I_{sd} > 0$. Bias voltage V on the TJ effectively scans f_s relatively to the studied f. (c), (e) Corresponding I-V curve and current noise of the TJ. The thin dotted line shows the standard shot-noise curve with equilibrium FD distribution in the wire. (f) Colored SEM micrograph of the device D1. The red cross indicates the position of the TJ used for sensing of ED located at one-quarter distance between two reservoirs.

Consider, for simplicity, the case of negligible inelastic scattering in the studied wire achieved at low enough T_0. Upon the application of a transport current I_{sd} through the wire, ED $f(\varepsilon)$ acquires an intermediate step, see Fig. 1(d) with the height depending linearly on the position along the wire [16]. At bias voltages V when the step in FD distribution f_s crosses the steps in f, the derivative dS_I/dV changes its value, which is expressed as two kinks in the $S_I(V)$ dependence, see Fig. 1(e). The presence of electron-electron (*e-e*) scattering in the wire leads to the smoothing of the kinks.

The colored SEM image of a typical device is presented in Fig. 1(f). The 3-μm-long 25-nm-thick and 100-nm-wide copper wire (brown) is evaporated above 20-nm-thick Al electrodes (blue) which were first controllably oxidized for 2 min with pure oxygen pressure of 1 mbar to form a TJ (red cross). The wire is well coupled to two thicker side aluminum reservoirs which are 125-nm-thick and were intentionally made as wide as possible [9]. These reservoirs are used to turn the wire out of equilibrium with a transport current I_{sd}. For sensing purposes, we used an Al electrode located either at one-quarter distance between two reservoirs (device D1) or in the middle of the wire (device D2). The unused Al electrode on both devices was left unbonded. The typical TJ resistance is around 25–30 kΩ, by far exceeding the sum of the wire's resistance (27 Ω) and its reservoir resistance ($\approx 1\,\Omega$ to the ground), ensuring negligible heat leakage to the sensor reservoir. To avoid any superconducting effects of Al electrodes, during the noise measurements we applied a perpendicular magnetic field at least sufficient to completely
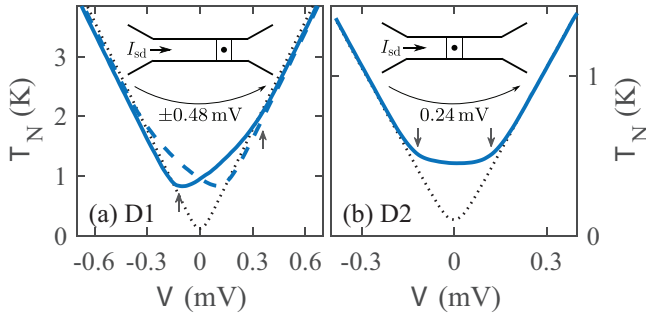
FIG. 2. Noise temperature vs bias voltage for the TJs realized at two different positions along the wire at $T_{\text{bath}} = 30\,\text{mK}$ in a magnetic field of $B = 5\,\text{T}$. (a) In the asymmetric case, T_{N} depends on the polarity of I_{sd} in accordance with Fig. 1(f), reflecting the locality of the extracted ED. (b) T_{N} is symmetric for the central positioning of the TJ. Dotted lines in both panels demonstrate T_{N} measured at $I_{\text{sd}} = 0$.

suppress superconductivity (120 mT). In a similar fashion, we also studied ED in the middle of 3-μm-long, 25-nm-thick, and 150-nm-wide Al wire realized in an all-aluminum TJ device (device D3, see Appendix A) with TJ resistance of 5 kΩ and the wire's resistance of 10 Ω. The noise measurement details, conventional transport, and noise properties of the TJs are described in Appendices A and B.

Knowledge of the Fano factor of the TJ allows one to infer $f(eV) = 1/2 - (1/F)d(k_{\text{B}}T_{\text{N}})/d(eV)$, where $T_{\text{N}} = S_I R_{\text{T}}/4k_{\text{B}}$ is the TJ's noise temperature and R_{T} is its resistance. This relation is valid when $k_{\text{B}}T_0$ is much less than the characteristic energy scale on which the local ED $f(\varepsilon)$ changes significantly. Figure 2 demonstrates the dependence $T_{\text{N}}(V)$ in devices D1 and D2 in large magnetic field 5 T. The dotted lines in panels (a) and (b) are measured in the absence of nonequilibrium in the metallic wire, $I_{\text{sd}} = 0$. In this case, the $T_{\text{N}}(V)$ dependence is typical: It is symmetric with respect to the V inversion and displays the parabolic transition from the Johnson-Nyquist noise at low $|V|$ to the linear shot noise at higher $|V|$. The finite transport current I_{sd} changes $T_{\text{N}}(V)$ drastically, see solid lines. For the TJ realized one-quarter of the way between two reservoirs, Fig. 2(a), $T_{\text{N}}(V)$ becomes asymmetric with kinklike features at $V = \mp V_{\text{sd}}/4$ and $V = \pm 3V_{\text{sd}}/4$ with upper signs corresponding to $I_{\text{sd}} > 0$ and lower signs corresponding to $I_{\text{sd}} < 0$. These features coincide with the expected kink positions, as indicated by arrows in Fig. 2(a) for $I_{\text{sd}} > 0$. In the case when the TJ is realized in the middle of the nonequilibrium conductor, Fig. 2(b), the $T_{\text{N}}(V)$ dependence is symmetric, however, with a near-zero bias plateaulike region. Note how this observation illustrates Eq. (1): Scanning the 1/2-plateau in $f(\varepsilon)$ with bias voltage V doesn't change T_{N}. Here, again, the plateau's boundaries coincide with expected kinks position, see arrows in Fig. 2(b). Overall, Fig. 2 reveals energy and spatial sensitivity of our approach. Note that similarly looking results were obtained for the noise measurements in a two-terminal TJ under biharmonic illumination [20] revealing the effect of interference of the two Fermi seas on both sides of the TJ. The proposed interpretation in terms of EDs, however, is unclear since both Fermi seas are equally important for the creation of the nonequilibrium and are equivalent with
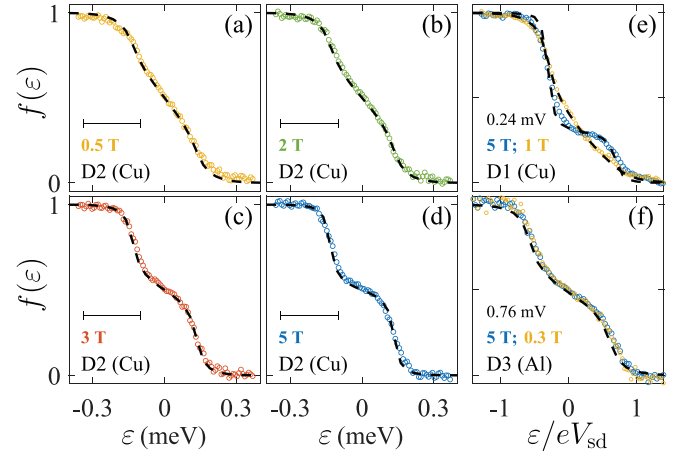

FIG. 3. (a)–(d) Magnetic field evolution of ED in the middle of the Cu wire (device D2) at $V_{\text{sd}} = 0.24\,\text{mV}$ (scale bar). Panel (d) corresponds to the data of Fig. 2(b). (e) ED in the Cu wire (device D1) at one-quarter distance between two reservoirs at $V_{\text{sd}} = 0.24\,\text{mV}$ (scale bar). (f) ED in Al device D3 at $V_{\text{sd}} = 0.76\,\text{mV}$. All the data are obtained at $T_{\text{bath}} = 30\,\text{mK}$. The dashed lines are solutions of the Boltzmann equation which fit the experimental EDs best.

respect to the applied ac excitation. On the contrary, in our case, nonequilibrium is created exclusively on one side of the TJ while the other reservoir remains in equilibrium and plays the role of a noninvasive sensor.

For data similar to that of Fig. 2, we are able to directly extract the local ED in the nonequilibrium situation. The results are summarized in Fig 3. Panels (a)–(d) present the evolution of ED as a function of the external magnetic field B at $I_{\text{sd}} = 9\,\mu\text{A}$ with the expected step width $V_{\text{sd}} = 0.24\,\text{mV}$ drawn by a scale bar. Remarkably, the expected double-step feature in the local ED is clearly seen for $B \geqslant 3\,\text{T}$ and completely smeared in low B-field. This manifests a B-dependent thermalization of electrons owing to an inelastic scattering process that can be suppressed by the magnetic field. Such behavior is not expected for the electron-phonon scattering, which is negligible anyway in our devices up to $V_{\text{sd}} \approx 1\,\text{mV}$ at $T_0 = 30\,\text{mK}$, see Appendix C, Fig. 8. Our result therefore demonstrates the impact of a magnetic field on the e-e scattering, which gradually diminishes at increasing B. This evolution persists up to $B \sim 5\,\text{T}$, where the effect of magnetic field saturates. Similar behavior is known from Refs. [29,40], where it was deduced from the features in differential conductance of a TJ due to Coulomb blockade utilizing the special design of the sensor electrode. The observed behavior is consistent with the presence of dilute magnetic impurities [41,42]—impurity-induced energy exchange in small magnetic fields freezes out at increasing B. Alternatively, the similar effect might also result from the presence of paramagnetic oxygen at the copper film surface [43].

Figure 3(e) demonstrates EDs at one-quarter distance between two reservoirs in a copper device D1 measured at $T_0 = 30\,\text{mK}$ for two representative values of a B field. Again, the step feature is almost indistinguishable in a smaller field $B = 1\,\text{T}$, however, the ED is far from the thermal one. As in D2, ED evolves with increasing B reaching saturation in $\sim 5\,\text{T}$. In Fig. 3(f), we demonstrate the ED in the middle of aluminum
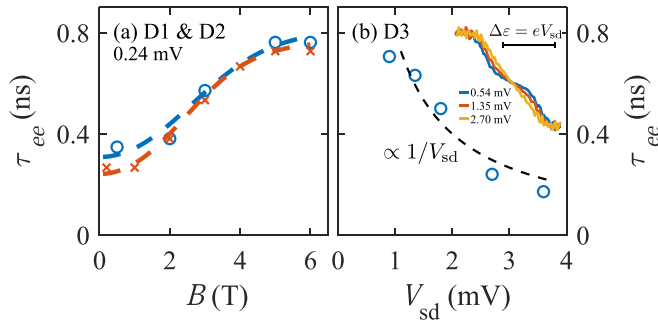
FIG. 4. (a) Scattering time as a function of magnetic field in devices D1 (crosses) and D2 (circles) at $V_{sd} = 0.24$ mV. The dashed lines effective temperatures are $T^*/(eV_{sd}/k_B) = 0.46$ and 0.39, correspondingly. (b) Scattering time as a function of V_{sd} in device D3 in $B = 5$ T. The inset demonstrates thermalization of ED at increasing bias voltage.

device D3, similarly obtained at two values of magnetic field. Unlike the case of copper, here the ED is independent of the magnetic field [44] and is of a double-step form already in small B. We note that it is also observable at higher $T_{bath} = 0.5$ K (see Appendix D Fig. 9). While the surface aluminum atoms may form a bath of magnetic moments [45] similar to the copper case, the observed difference between two materials may indicate a smaller density of the magnetic moments and/or their weaker coupling to the conduction electrons in aluminum.

Extracted EDs provide access to *e-e* scattering time in the copper wires as a function of B. The ED inside a quasi-one-dimensional conductor obeys the Boltzmann equation [46,47] $D\partial^2 f(x, E)/\partial x^2 + I_{coll}(x, E, \{f\}) = 0$. Here, $D = L^2/\tau_D$ is the diffusion coefficient, L – length of the wire, τ_D is the diffusion time of electrons along the wire, and x is the coordinate along the wire. Taking into account only *e-e* scattering and assuming the interaction is local, one gets $I_{coll}(x, E, \{f\}) = \int d\varepsilon \, dE' K(\varepsilon) f^x_{E'}(1 - f^x_{E'+\varepsilon}) \times [(1 - f^x_E)f^x_{E+\varepsilon} - f^x_E(1 - f^x_{E-\varepsilon})]$, where $K(\varepsilon)$ is the interaction kernel. The dominant role of exchange interaction of electrons with magnetic impurities suggests $K(\varepsilon) = \tau_{ee}^{-1}/\varepsilon^2$, where τ_{ee}^{-1} is the rate of *e-e* scattering [27,41]. Using the numerical relaxation method, we solve the Boltzmann equation and obtain the ratio τ_{ee}/τ_D which fits the experimental EDs best. Corresponding best fits are shown by dashed lines in Fig. 3.

In Fig. 4(a), we plot the obtained τ_{ee} in dependence of the magnetic field for both copper devices, see the symbols. At increasing B from 0.3 T to 6 T τ_{ee} grows monotonically and saturates at high B. This evolution may be understood as follows. For the B-dependent *e-e* scattering rate, we assume $1/\tau_{ee}(B) = 1/\tau_{sf}(B) + 1/\tau_0$, where τ_{sf} is the spin-flip rate due to B-dependent scattering involving magnetic impurities, and τ_0 is the B-independent scattering rate, e.g., due to the direct Coulomb interaction. For the spin-flip rate, we use the expression similar to that in thermal equilibrium [48] $\tau_{sf}(B)/\tau_{sf}(B=0) = \sinh(g\mu_B B/k_B T^*)/(g\mu_B B/k_B T^*)$, where μ_B is the Bohr magneton, g is the gyromagnetic factor of the magnetic impurities. The effective temperature in our strongly nonequilibrium case should scale with the bias voltage on the metallic wire $T^* \sim eV_{sd}/k_B$. This expression closely describes

our data, assuming $g = 2$, $T^*/(eV_{sd}/k_B) = 0.46$ and 0.39 and $\tau_0/\tau_D = 1.02$ and 0.96, respectively, for devices D1 and D2. We compare the obtained values for τ_{ee} with the theoretical prediction of Refs. [49,50] in Appendix E.

We note that, experimentally, the double-step feature smooths out at increasing V_{sd}. This is illustrated in the inset of Fig. 4(b), where EDs measured in D3 are plotted as functions of the normalized energy $\varepsilon/(eV_{sd})$ for various values of V_{sd}. Smoothing of EDs is an obvious consequence of the direct Coulomb interaction which starts to dominate at increasing excess quasiparticle energy. For the kernel of Coulomb interaction, $K_{Coulomb}(\varepsilon) \propto \varepsilon^{-3/2} \tau_0$ depends on the exact ED [50] which, in turn, depends both on the energy of the quasiparticle and on the position along the wire. To estimate τ_{ee}, we formally use the same kernel as before, however, with the bias-dependent scattering time $K(\varepsilon) = \tau_{ee}^{-1}(V_{sd})/\varepsilon^2$. For device D3, the results are shown in Fig. 4(b). The dependence $\tau_{ee}(V_{sd})$ is stronger than that expected in 1D [50] $\tau_{ee} \propto V_{sd}^{-1/2}$, probably indicating the transition of the wire to effectively larger dimensionality in terms of energy relaxation.

We note that the demonstrated approach is also applicable to the study of nonequilibrium configurations associated with spin (or valley, etc.) currents. Naturally, in this case the local noise probe should additionally conserve the respective quantum number. Theoretically, it is known that the current noise reflects the degree of spin imbalance in the reservoirs [51]. Experimentally, this concept was recently investigated in the study of the spin accumulation driven shot noise across a tunnel barrier with a spin-polarized injection contact [52]. In this respect, potentially, our approach may be useful for investigating the microscopic details of spin (or valley, etc.) relaxation.

In summary, we experimentally demonstrated the local sensing of the nonequilibrium ED in a diffusive metallic wire based on shot-noise measurements with a TJ. This approach relies solely on the Pauli exclusion principle and works in the absence of the energy-selective features in conductance. Consequently, the energy resolution of such a measurement is only limited by the bath temperature. The spatial resolution is virtually unlimited with state-of-the-art noise scanning techniques [6,53–55]. The approach is quite universal and equally suitable for the measurements of the nonequilibrium configurations created by charge, spin [56] and valley, etc. currents, hence paving the way for the realization of existing [26,36,37,57] and various novel local noise probes.
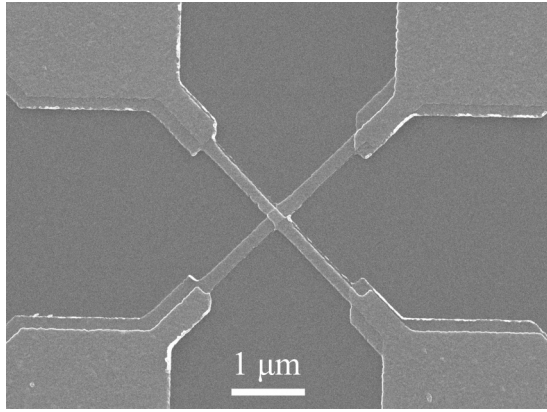
FIG. 5. SEM microphotograph of device D3. All-aluminum TJ (in the middle) is realized between 3μm-long, 25-nm-thick, and 150 nm-wide Al wires.

We thank H. Pothier, I. L. Aleiner and A. D. Zaikin for helpful discussions.

APPENDIX A: DEVICE AND MEASUREMENT TECHNIQUES

The colored SEM image of device D3 is presented in Fig. 5. To characterize our devices in terms of the electronic elastic mean-free path (mfp), we do as follows. The diffusion coefficient D is first obtained from the Einstein's relation $\sigma = v_F e^2 D$. Then, the mfp is obtained from $D = 1/3 v_F l$ with v_F the Fermi velocity. For Cu devices D1 and D2, we find $D = 120 \, \text{cm}^2/\text{s}$, $\tau_D = 0.8 \, \text{ns}$, $l_{\text{mfp}} = 23 \, \text{nm}$; for Al device D3— $D = 200 \, \text{cm}^2/\text{s}$, $\tau_D = 1.2 \, \text{ns}$, $l_{\text{mfp}} = 30 \, \text{nm}$.

The noise spectral density was measured using a homemade low-temperature amplifier (LTamp) with a voltage gain of about 10 dB and input current noise of ~ 2–$6 \times 10^{-27} \, \text{A}^2/\text{Hz}$. The voltage fluctuations on a $6.4 \, \text{k}\Omega$ load resistor were measured near the central frequency 7 MHz of a resonant circuit at the input of the LTAmp. The output of the LTamp was fed into the low noise 75 dB gain room-temperature amplification stage followed by a handmade ana-
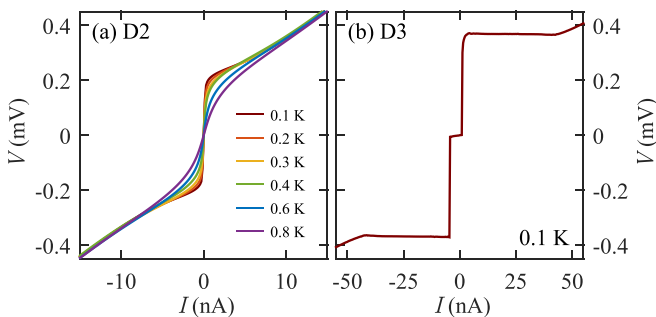

FIG. 6. I-V curves of the copper and aluminum devices. (a) In D2, the I-V characteristics of the TJ in $B = 0$ demonstrates the typical NIS behavior with drastic decrease of subgap conductance with decreasing temperature, and conductance peaks at $\sim 190 \, \mu$eV, reflecting the maxima in the density of states of the superconducting Al. (b) In D3, the I-V curve in $B = 0$ demonstrates the typical SIS behavior.
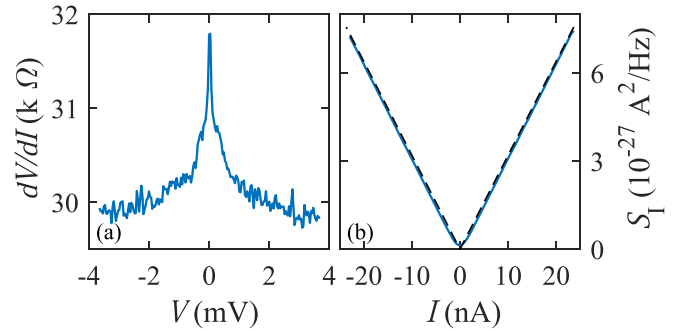

FIG. 7. Differential resistance and shot noise of the tunnel junction. (a) Differential resistance and (b) shot noise of the tunnel junction in the device D1 measured at $T_{\text{bath}} = 30 \, \text{mK}$ in $B = 0.3 \, \text{T}$. The nonlinearity of dV/dI is approximately 5%.

log filter and a power detector. The setup was calibrated using the equilibrium Johnson-Nyquist noise thermometry. Unless otherwise stated, the measurements were performed in a cryogen-free Bluefors dilution refrigerator BF-LD250 at a bath temperature of 30 mK.

APPENDIX B: TRANSPORT AND NOISE PROPERTIES OF THE TJS

For all three devices, we first characterize the TJs in terms of conventional transport and noise properties. For devices D1 and D2, the I-V characteristics in $B = 0$ demonstrated the typical normal metal-insulator-superconductor (NIS) behavior with drastic decrease of subgap conductance with decreasing temperature, and conductance peaks at $\sim 190 \, \mu$eV, reflecting the maxima in the density of states of the superconducting Al. The device D3 showed the typical SIS behavior (see Fig. 6 for the I-V curves of both devices). All three devices demonstrated almost linear I-V curves in finite magnetic field suppressing superconductivity with negligible contribution of interaction effects [58] (see Fig. 7). In terms of noise in the normal state, devices D1 and D3 demonstrated the standard
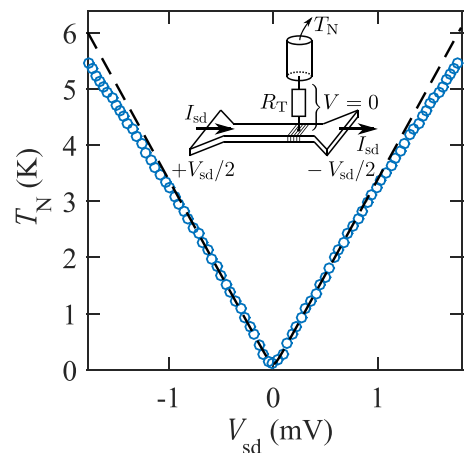

FIG. 8. Local noise measurement in the Cu strip. The inset shows the measurement scheme. Data in 0.3 T and in 6 T (circles) are almost indistinguishable. The dashed curve is a fit for the absent electron-phonon scattering in the strip.
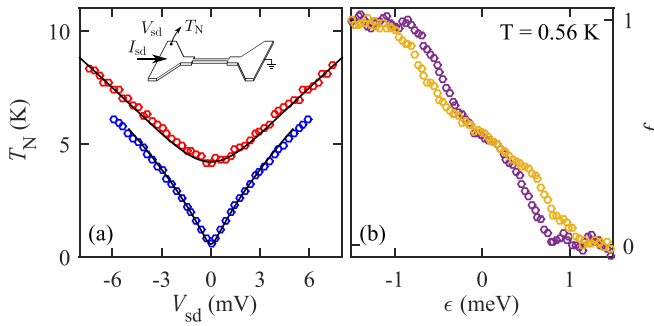
FIG. 9. Average and local noise measurements in the Al strip. (a) Symbols: Average noise temperature as a function of bias voltage across the heater at $T = 4.2$ K (red) and $T = 0.56$ K (blue). Numerical simulation taking into account geometry of the sample is shown by solid lines. (b) ED in Al wire at $T = 0.56$ K at $V_{sd} = 1.2$ mV (violet) and $V_{sd} = 1.8$ mV (yellow). The measurements are performed in the ^{3}He insert.

Fano-factor $F = 1$, common for TJs. In device D2, we measured a linear behavior typical for TJs, however, with $F = 0.6$ which might be a result of a pinhole. This junction also acts as a current noise-to-ED converter, yet with a slightly smaller sensitivity owing to the reduced shot noise.

APPENDIX C: PHONONS

The linear dependence $T_N(V_{sd})$ at $V_{sd} \lesssim 1$ meV at $T_{bath} = 30$ mK (see Fig. 8) demonstrates the absence of *e-ph* energy relaxation at corresponding excess energies of quasiparticles (qp's). At higher qp energies, the $T_N(V_{sd})$-dependence becomes sublinear, indicating the power flow from the electron system to the phonon one.

APPENDIX D: AVERAGE AND LOCAL NOISE MEASUREMENTS IN THE AL STRIP AT 0.56 K

Numerical simulation taking into account geometry of the sample fits experimental data, see Fig. 9(a), for $\Sigma_{e\text{-ph}} = 2.3 \times 10^{11}$ W/m^{3}K^3. This value allows one to estimate the *e-ph*

scattering length $l_{e\text{-ph}} = \sqrt{(\sigma \mathcal{L})/(3\Sigma_{e\text{-ph}}T)}$ to be $2.3\,\mu$m at $T_{bath} = 0.56$ K, which is only slightly less than the length of the constriction $l = 3\,\mu$m. This fact allows the observation of double-step feature at $T_{bath} = 0.56$ K as shown in Fig. 9(b). In the simulation, electronic heat conduction is assumed to satisfy the Wiedemann-Franz law $\varkappa = \sigma \mathcal{L}T$, where $\mathcal{L} = (\pi^2/3)(k_B/e)^2 = 2.44 \times 10^{-8}\,W\Omega K^{-2}$ is the Lorenz number.

APPENDIX E: ENERGY RELAXATION TIME ESTIMATION

According to Ref. [50], energy relaxation time in a 1D case is given by

$$\frac{\hbar}{\tau_E} = \frac{e^2}{\hbar} \frac{L_\varepsilon}{\sigma_1} \varepsilon, \qquad L_\varepsilon = \sqrt{\frac{\hbar D}{\varepsilon}},$$

where σ_1 is the 1D conductivity. For our copper wires, using $D = 120$ cm^2/s and $\sigma_1 = 10^{-7}$ m/Ω, we estimate (at $\varepsilon = 0.24$ meV)

$$\tau_E \approx 6\,\text{ns}, \qquad L_\varepsilon \approx 200\,\text{nm}.$$

The contribution from the triplet channel (spin density fluctuations) is practically of the same value and may further decrease τ_E, making it comparable to the experimental value.

APPENDIX F: APPLICABILITY OF THE APPROACH

Overall, the data presented in the main text is evidence of the power of the local shot-noise measurement for the energy resolution of the electronic states out of equilibrium. There are two necessary conditions for this approach to work. One is the elasticity of charge transport through the TJ, which would then preserve spectral information. The second one requires the much smaller thermal conductance of the TJ compared to that of the studied conductor [33,38,39,57,59], similarly to the analogous electrical requirement for conventional volt meters. To probe low-resistance conductors, these conditions, alongside TJs, are fulfilled for elastic InAs nanowire-based sensors, allowing additionally thermoelectric or spin-to-charge conversion studies [56,57].

[1] G. Kucsko, P. C. Maurer, N. Y. Yao, M. Kubo, H. J. Noh, P. K. Lo, H. Park, and M. D. Lukin, Nature **500**, 54 (2013).

[2] D. Halbertal, J. Cuppens, M. B. Shalom, L. Embon, N. Shadmi, Y. Anahory, H. R. Naren, J. Sarkar, A. Uri, Y. Ronen, Y. Myasoedov, L. S. Levitov, E. Joselevich, A. K. Geim, and E. Zeldov, Nature **539**, 407 (2016).

[3] F. Menges, P. Mensch, H. Schmid, H. Riel, A. Stemmer, and B. Gotsmann, Nat. Commun. **7**, 10874 (2016).

[4] S. Kolkowitz, A. Safira, A. A. High, R. C. Devlin, S. Choi, Q. P. Unterreithmeier, D. Patterson, A. S. Zibrov, V. E. Manucharyan, H. Park, and M. D. Lukin, Science **347**, 1129 (2015).

[5] L. Spietz, Science **300**, 1929 (2003).

[6] U. Kemiktarak, T. Ndukum, K. C. Schwab, and K. L. Ekinci, Nature **450**, 85 (2007).

[7] M. L. Roukes, M. R. Freeman, R. S. Germain, R. C. Richardson, and M. B. Ketchen, Phys. Rev. Lett. **55**, 422 (1985).

[8] A. H. Steinbach, J. M. Martinis, and M. H. Devoret, Phys. Rev. Lett. **76**, 3806 (1996).

[9] M. Henny, S. Oberholzer, C. Strunk, and C. Schönenberger, Phys. Rev. B **59**, 2871 (1999).

[10] A. C. Betz, F. Vialla, D. Brunel, C. Voisin, M. Picher, A. Cavanna, A. Madouri, G. Fève, J.-M. Berroir, B. Plaçais, and E. Pallecchi, Phys. Rev. Lett. **109**, 056805 (2012).

[11] A. C. Betz, S. H. Jhang, E. Pallecchi, R. Ferreira, G. Fève, J.-M. Berroir, and B. Plaçais, Nat. Phys. **9**, 109 (2012).

[12] K. C. Fong, E. E. Wollman, H. Ravi, W. Chen, A. A. Clerk, M. D. Shaw, H. G. Leduc, and K. C. Schwab, Phys. Rev. X **3**, 041008 (2013).

[13] A. Laitinen, M. Kumar, M. Oksanen, B. Plaçais, P. Virtanen, and P. Hakonen, Phys. Rev. B **91**, 121414(R) (2015).

[14] C. B. McKitterick, D. E. Prober, and M. J. Rooks, Phys. Rev. B **93**, 075410 (2016).

[15] S. Zihlmann, P. Makk, S. Castilla, J. Gramich, K. Thodkar, S. Caneva, R. Wang, S. Hofmann, and C. Schönenberger, Phys. Rev. B **99**, 075419 (2019).

[16] K. Nagaev, Phys. Lett. A **169**, 103 (1992).

[17] Y. Blanter and M. Büttiker, Phys. Rep. **336**, 1 (2000).

[18] G. B. Lesovik and L. S. Levitov, Phys. Rev. Lett. **72**, 538 (1994).

[19] R. J. Schoelkopf, A. A. Kozhevnikov, D. E. Prober, and M. J. Rooks, Phys. Rev. Lett. **80**, 2437 (1998).

[20] J. Gabelli and B. Reulet, Phys. Rev. B **87**, 075403 (2013).

[21] E. Pinsolle, A. Rousseau, C. Lupien, and B. Reulet, Phys. Rev. Lett. **116**, 236601 (2016).

[22] H. Inoue, A. Grivnin, N. Ofek, I. Neder, M. Heiblum, V. Umansky, and D. Mahalu, Phys. Rev. Lett. **112**, 166801 (2014).

[23] T. Jullien, P. Roulleau, B. Roche, A. Cavanna, Y. Jin, and D. C. Glattli, Nature **514**, 603 (2014).

[24] R. Bisognin, A. Marguerite, B. Roussel, M. Kumar, C. Cabart, C. Chapdelaine, A. Mohammad-Djafari, J.-M. Berroir, E. Bocquillon, B. Plaçais, A. Cavanna, U. Gennser, Y. Jin, P. Degiovanni, and G. Fève, Nat. Commun. **10**, 3379 (2019).

[25] J. Keeling, I. Klich, and L. S. Levitov, Phys. Rev. Lett. **97**, 116403 (2006).

[26] T. Gramespacher and M. Büttiker, Phys. Rev. B **60**, 2375 (1999).

[27] H. Pothier, S. Guéron, N. O. Birge, D. Esteve, and M. H. Devoret, Phys. Rev. Lett. **79**, 3490 (1997).

[28] F. Pierre, A. Anthore, H. Pothier, C. Urbina, and D. Esteve, Phys. Rev. Lett. **86**, 1078 (2001).

[29] A. Anthore, F. Pierre, H. Pothier, and D. Esteve, Phys. Rev. Lett. **90**, 076806 (2003).

[30] Y.-F. Chen, T. Dirks, G. Al-Zoubi, N. O. Birge, and N. Mason, Phys. Rev. Lett. **102**, 036804 (2009).

[31] C. Altimiras, H. le Sueur, U. Gennser, A. Cavanna, D. Mailly, and F. Pierre, Nat. Phys. **6**, 34 (2009).

[32] K. Itoh, R. Nakazawa, T. Ota, M. Hashisaka, K. Muraki, and T. Fujisawa, Phys. Rev. Lett. **120**, 197701 (2018).

[33] E. S. Tikhonov, D. V. Shovkun, D. Ercolani, F. Rossella, M. Rocci, L. Sorba, S. Roddaro, and V. S. Khrapai, Sci. Rep. **6**, 30621 (2016).

[34] O. S. Lumbroso, L. Simine, A. Nitzan, D. Segal, and O. Tal, Nature **562**, 240 (2018).

[35] G. Cabra, M. Di Ventra, and M. Galperin, Phys. Rev. B **98**, 235432 (2018).

[36] J. Kühne, I. Protopopov, Y. Oreg, and A. Mirlin, Physica E **82**, 293 (2016).

[37] T. Ota, M. Hashisaka, K. Muraki, and T. Fujisawa, J. Phys.: Condens. Matter **29**, 225302 (2017).

[38] S. Piatrusha and V. Khrapai, in *2017 International Conference on Noise and Fluctuations (ICNF), Vilnius, 2017* (IEEE, 2017), pp. 1–4.

[39] A. O. Denisov, E. S. Tikhonov, S. U. Piatrusha, I. N. Khrapach, F. Rossella, M. Rocci, L. Sorba, S. Roddaro, and V. S. Khrapai, Nanotechnology **31**, 324004 (2020).

[40] B. Huard, A. Anthore, N. O. Birge, H. Pothier, and D. Esteve, Phys. Rev. Lett. **95**, 036802 (2005).

[41] A. Kaminski and L. I. Glazman, Phys. Rev. Lett. **86**, 2400 (2001).

[42] G. Göppert, Y. M. Galperin, B. L. Altshuler, and H. Grabert, Phys. Rev. B **66**, 195328 (2002).

[43] J. Vranken, C. Van Haesendonck, and Y. Bruynseraede, Phys. Rev. B **37**, 8502 (1988).

[44] A. Anthore, Decoherence mechanisms in mesocopic conductors, Ph.D. thesis, Université Pierre et Marie Curie–Paris VI, 2003.

[45] D. Lee, J. L. DuBois, and V. Lordi, Phys. Rev. Lett. **112**, 017001 (2014).

[46] K. E. Nagaev, Phys. Rev. B **52**, 4740 (1995).

[47] V. I. Kozub and A. M. Rudin, Phys. Rev. B **52**, 7853 (1995).

[48] F. Pierre, A. B. Gougam, A. Anthore, H. Pothier, D. Esteve, and N. O. Birge, Phys. Rev. B **68**, 085413 (2003).

[49] B. L. Altshuler, A. G. Aronov, and D. E. Khmelnitsky, J. Phys. C **15**, 7367 (1982).

[50] I. L. Aleiner and Y. M. Blanter, Phys. Rev. B **65**, 115317 (2002).

[51] J. Meair, P. Stano, and P. Jacquod, Phys. Rev. B **84**, 073302 (2011).

[52] T. Arakawa, J. Shiogai, M. Ciorga, M. Utz, D. Schuh, M. Kohda, J. Nitta, D. Bougeard, D. Weiss, T. Ono, and K. Kobayashi, Phys. Rev. Lett. **114**, 016601 (2015).

[53] H. Birk, M. J. M. de Jong, and C. Schönenberger, Phys. Rev. Lett. **75**, 1610 (1995).

[54] F. Massee, Q. Dong, A. Cavanna, Y. Jin, and M. Aprili, Rev. Sci. Instrum. **89**, 093708 (2018).

[55] K. M. Bastiaans, D. Cho, D. Chatzopoulos, M. Leeuwenhoek, C. Koks, and M. P. Allan, Phys. Rev. B **100**, 104506 (2019).

[56] V. S. Khrapai and K. E. Nagaev, JETP Letters **105**, 18 (2017).

[57] E. S. Tikhonov, D. V. Shovkun, D. Ercolani, F. Rossella, M. Rocci, L. Sorba, S. Roddaro, and V. S. Khrapai, Semicond. Sci. Technol. **31**, 104001 (2016).

[58] A. D. Zaikin and D. S. Golubev, in *Dissipative Quantum Mechanics of Nanostructures*, edited by A. D. Zaikin and D. Golubev (Jenny Stanford Publishing, Singapore, 2019).

[59] S. Larocque, E. Pinsolle, C. Lupien, and B. Reulet, arXiv:2002.10339 [cond-mat.mes-hall].